Archives of Advances in Biosciences

Original Article

Iron-doped boron nitride nanocage for targeted delivery of 5 fluorouracil: A DFT guided experimental study with in vitro validation

Sara Sandi[1], Abolghasem Shameli[2], Maziar Noei[1], Ebrahim Balali [3*], Mahmoud Mirzaei [4,5]

[1.] Department of Pharmaceutical Chemistry, TeMS.C., Islamic Azad University, Tehran, Iran.
[2.] Department of chemistry, Om.C. , Islamic Azad University, Omidiyeh, Iran.
[3.] Department of Organic Chemistry, TeMS.C., Islamic Azad University, Tehran, Iran. Email: ebrahim.balali@iau.ac.ir
[4.] Department of Physics, Faculty of Science, Arak University, Arak, Iran.
[5.] Laboratory of Molecular Computations (LMC), Department of Natural and Mathematical Sciences, Faculty of Engineering, Tarsus University, Tarsus, Turkiye.

Received: 19 May 2026; **Accepted:** 29 Jun 2026; **Published:** 15 Jul 2026

Cite this article as: Sandi, S., Shameli, A., Noei, M., & Balali, E. Mirzaei, M. Iron-doped boron nitride nanocage for targeted delivery of 5 fluorouracil: A DFT guided experimental study with in vitro validation. Archives of Advances in Biosciences. 2026 17(1):1-17. https://doi.org/10.22037/aab.v16i1.52105

Abstract

Background and Aim: 5-Fluorouracil (5-FU) is a widely used anticancer drug but suffers from severe systemic toxicity, short half-life, and low tumor selectivity. Boron nitride nanocages have emerged as promising drug delivery vehicles due to their high biocompatibility and low cytotoxicity. Transition metal doping, particularly with iron, can enhance drug binding affinity through electronic effects.

The purpose of this study was to evaluate the potential of iron-doped boron nitride nanocage (NC Fe) as a nanocarrier for targeted delivery of 5-FU using a multiscale approach combining DFT calculations, experimental adsorption studies, and in vitro cellular/molecular assays.

Methods: DFT calculations at the B3LYP/6 31G(d) level were performed to determine the interaction energy, QTAIM parameters, NBO charge transfer, and HOMO LUMO gap of the FU-NC-Fe complex. Batch adsorption experiments were conducted to optimize pH, contact time, initial drug concentration, and adsorbent dosage. MTT assay, flow cytometry (Annexin V FITC/PI staining), and qRT-PCR (Bax and Bcl-2 expression) were performed on MCF-7 breast cancer cells and normal HFF fibroblasts.

Results: DFT calculations revealed a negative interaction energy of –59.8 kJ/mol with positive $\nabla^2\rho(r)$ (0.098 a.u.), confirming spontaneous noncovalent binding. Bidirectional charge transfer of 0.29 electrons and an 11.8% reduction in HOMO LUMO gap were observed. Optimal adsorption conditions (pH 7.0, 30 min, 20 mg/L, 0.10 g NC Fe) yielded 76.5% adsorption efficiency. FU-NC-Fe exhibited significantly enhanced cytotoxicity against MCF- 7 cells (IC_{50} = 8.7 µg/mL) compared to free 5-FU (18.4 µg/mL), with a selectivity index of 4.86. The complex induced 52.7% total apoptosis (vs. 28.4% for free drug) and increased the Bax/Bcl-2 ratio 4.5 fold (21.3 vs. 4.7). Pristine NC-Fe showed excellent biocompatibility (IC_{50} > 200 µg/mL).

Conclusion: Iron-doped boron nitride nanocage is a highly promising nanocarrier for targeted 5-FU delivery, offering enhanced anticancer efficacy, high cancer cell selectivity, and potent apoptosis induction through the mitochondrial pathway.

Keywords: 5-Fluorouracil, Boron nitride nanocage, Iron doping, Drug delivery, DFT, Breast cancer, Apoptosis

1. Introduction

Cancer is currently recognized as one of the most serious global health threats. Statistical data from the World Health Organization show that approximately 19.3 million new cancer cases were diagnosed worldwide in 2020, and nearly 10 million patients died from this disease (1). The main challenge in cancer therapy is not only the aggressive nature of malignant cells but also the severe side effects associated with conventional chemotherapeutic drugs (2). Although these agents are effective against rapidly dividing tumor cells, they also affect healthy tissues, such as bone marrow, gastrointestinal epithelium, and hair follicles, resulting in dose limiting toxicities (3).

Among the most widely prescribed anticancer drugs, 5-fluorouracil (5-FU) has remained a standard for the treatment of colorectal, breast, gastric, and head/neck cancers for more than six decades (4). The mechanism of action of 5-FU involves inhibition of thymidylate synthase, which disrupts DNA synthesis and leads to cell death (5). However, clinical application of free 5-FU is limited by significant drawbacks, including a short plasma half-life (approximately 10–20 minutes), poor oral bioavailability, the development of drug resistance, and serious adverse effects such as cardiotoxicity and myelosuppression (6, 7). These limitations have motivated researchers to seek more effective and safer delivery systems for this valuable drug.

Nanotechnology offers promising solutions to overcome the aforementioned challenges (8). Various nanocarriers including liposomes, polymeric nanoparticles, dendrimers, and carbon based nanomaterials, have been investigated for targeted drug delivery (9). Among these, boron nitride (BN) nanostructures have recently attracted considerable attention due to their unique combination of properties: high thermal and chemical stability, excellent biocompatibility, low cytotoxicity, and large surface area (10, 11). Unlike carbon nanotubes, which often exhibit significant toxicity, BN nanostructures show favorable interactions with biological systems, making them suitable for biomedical applications (12). Specifically, boron nitride nanocages (BNNCs) with the general formula $(BN)_{12}$ have been identified as promising drug carriers (13). These cage-like structures possess a hollow interior and a polar surface arising from alternating boron and nitrogen atoms with different electronegativities (14). The polarity of B–N bonds facilitates non-covalent interactions with drug molecules through electrostatic and van der Waals forces (15). Furthermore, the electronic properties of BN nanocages can be tuned by doping with foreign atoms, which involves substitution of boron or nitrogen atoms with other elements (16).

Previous theoretical studies have demonstrated that doping BN nanostructures with transition metals significantly enhances their interaction with various drug molecules (17, 18). In particular, iron (Fe) doping has been shown to increase the dipole moment and reactivity of BN nanocages, leading to stronger drug adsorption (19). Experimental investigations have also confirmed that iron-doped BN nanomaterials exhibit improved drug loading capacity and controlled-release behavior (20). However, to the best of our knowledge, a comprehensive study combining density functional theory (DFT) calculations, experimental adsorption measurements, and in vitro cellular assays for the specific system of 5-FU with an iron-doped BN nanocage (denoted as FU-NC-Fe) has not yet been reported.

The present study aims to fill this research gap through a multiscale approach. First, DFT calculations were performed to evaluate the interaction energy, charge transfer, and electronic properties of the FU-NC-Fe complex. Second, experimental adsorption studies were carried out to optimize key parameters, including pH, contact time, initial drug concentration, and adsorbent dosage. Third, in vitro cytotoxicity assays on MCF-7 breast cancer cells and molecular studies, including apoptosis detection and gene expression analysis, were conducted to assess the biological performance of the FU-NC-Fe system. The integrated findings provide a solid foundation for developing iron-doped BN nanocages as effective nanocarriers for targeted delivery of 5-fluorouracil.

2. Methods

2.1. Computational details (DFT)

All quantum chemical calculations were performed using the Gaussian 16 software package. The initial three-dimensional structures of 5-fluorouracil (5-FU) and the iron-doped boron nitride nanocage (NC-Fe, with the composition $B_{11}FeN_{12}$) were constructed using GaussView 6.0. The nanocage was built based on the $(BN)_{12}$ fullerene-like structure, in which one boron atom was substituted with an iron atom. Geometry optimizations of the isolated drug, the isolated nanocage, and the FU-NC-Fe complex were carried out using density functional theory (DFT) with the hybrid B3LYP functional and the 6-31G(d) basis set. This level of theory has been successfully applied to similar drug-nanocarrier systems (1,2). To account for dispersion interactions in this iron-containing system, single-point energy calculations were additionally performed using the B3LYP-D3 correction (Grimme's dispersion with Becke-Johnson damping) at the optimized geometries. The interaction energy obtained with B3LYP-D3 was –61.2 kJ/mol, which differs by only 2.3% from the B3LYP value (–59.8 kJ/mol), confirming that dispersion forces do not

play a dominant role in this system and that the B3LYP level of theory is sufficient for qualitative and semi-quantitative analysis. The spin state of the iron atom in NC-Fe was investigated by comparing the energies of different spin multiplicities. Geometry optimizations were performed for singlet (S = 0), triplet (S = 1), and quintet (S = 2) spin states. The triplet state (S = 1) was found to be the most stable, with an energy difference of 18.4 kJ/mol and 32.7 kJ/mol compared to the singlet and quintet states, respectively. Therefore, all calculations were performed with the iron atom in its triplet spin state.

To confirm that the optimized structures correspond to true local minima on the potential energy surface, harmonic vibrational frequency calculations were performed at the same level of theory. The absence of imaginary frequencies was verified for all optimized structures. The interaction energy (E_int) between 5-FU and NC-Fe was calculated according to the following equation:

E_int = E_complex – (E_drug + E_nanocage)

where E_complex is the total energy of the optimized FU-NC-Fe complex, and E_drug and E_nanocage are the total energies of the isolated 5-FU and NC-Fe, respectively (3). To account for the influence of the biological environment, single-point energy calculations were also performed using the polarizable continuum model (PCM) with water as the solvent.

Electronic properties, including the energies of the highest occupied molecular orbital (HOMO), the lowest unoccupied molecular orbital (LUMO), and the HOMO-LUMO energy gap (ΔE), were extracted from the optimized structures. Natural bond orbital (NBO) analysis was performed at the same level of theory to evaluate charge transfer between the drug and the nanocage. The quantum theory of atoms in molecules (QTAIM) was applied using the AIMAll package to analyze the nature of the interaction at the bond critical points (BCPs). The electron density $\rho(r)$ and its Laplacian $\nabla^2\rho(r)$ were computed at all BCPs between 5-FU and NC-Fe (4).

2.2. Experimental adsorption study

2.2.1. Materials

5-Fluorouracil (purity ≥ 99%) was purchased from Sigma Aldrich (Germany). Iron-doped boron nitride nanocage (NC-Fe, purity ≥ 98%, particle size 45 ± 5 nm, based on SEM analysis) was obtained from SinaZist (Iran). All other chemicals, including hydrochloric acid (HCl), sodium hydroxide (NaOH), phosphate buffer salts, and ethanol, were of analytical grade and obtained from Merck (Germany). Deionized water was used throughout the experiments.

2.2.2. Characterization

The morphology and surface topography of NC-Fe were examined using field-emission scanning electron microscopy (FE-SEM, TESCAN) at an accelerating voltage of 15 kV. Samples were sputter-coated with gold prior to imaging. The average particle size was determined from SEM images using ImageJ software (n = 100 particles).The hydrodynamic diameter and size distribution of NC-Fe dispersed in deionized water (0.1 mg/mL) were measured by dynamic light scattering (DLS) using a Malvern Zetasizer Nano ZS (Malvern Instruments, UK) at 25°C with a scattering angle of 173°. The zeta potential (ζ-potential) was determined by electrophoretic light scattering using the same instrument. All measurements were performed in triplicate. The crystalline structure of NC-Fe was analyzed by X-ray diffraction (XRD) using a Bruker D8 Advance diffractometer (Bruker) with Cu Kα radiation (λ = 1.5406 Å), operated at 40 kV and 40 mA. Data were collected over the 2θ range of 10–80° with a step size of 0.02° and a scan rate of 2°/min. Phase identification was performed by comparison with standard JCPDS reference patterns. Fourier-transform infrared (FTIR) spectroscopy was performed to identify the surface functional groups and chemical bonds of NC-Fe. The sample was mixed with KBr powder and pressed into a pellet. FTIR spectra were recorded in transmission mode using a PerkinElmer Spectrum Two spectrometer (PerkinElmer) over the wavenumber range of 400–4000 cm^{-1} with a resolution of 4 cm^{-1} and 32 scans per sample.

2.2.3. Preparation of calibration curve)

A stock solution of 5-FU (100 mg/L) was prepared by dissolving 10 mg of the drug in 100 mL of deionized water with the aid of sonication for 10 minutes. Working standard solutions at concentrations of 5, 10, 20, 50, and 100 mg/L were prepared by serial dilution of the stock solution. The maximum absorption wavelength (λ_max) of 5-FU was determined by scanning the 20 mg/L solution in the range of 200–400 nm using a UV-Vis spectrophotometer (UV-1800, Shimadzu, Japan). The absorbance of each standard solution was measured at λ_max = 266 nm, and the calibration curve (absorbance vs. concentration) was constructed by linear regression analysis (5).

2.2.3. Batch adsorption experiments

All adsorption experiments were carried out in 50 mL Erlenmeyer flasks with a working volume of 10 mL. For each experiment, a predetermined amount of NC-Fe was added to a 5-FU solution of known concentration. The pH of the solution was adjusted to the desired value using 0.1 M HCl or 0.1 M NaOH, measured by a digital pH meter (SevenCompact S220, Mettler-Toledo). The mixture was sonicated for 5 minutes to disperse the nanocage, then placed in an incubator shaker (ISF 1-V, Adolf Kühner, Switzerland) at 25°C and 150 rpm for a specified contact time. After the adsorption period, the solution was centrifuged at 4000 rpm for 15 minutes, and the

supernatant was filtered through a 0.22 µm syringe filter. The residual concentration of 5-FU in the filtrate was determined by UV-Vis spectrophotometry at 266 nm. All experiments were performed in triplicate, and results are reported as mean ± standard deviation (SD) (6).

In addition to adsorption percentage (R%) and adsorption capacity (q_e), three key drug-loading parameters were calculated to evaluate the performance of the NC-Fe nanocarrier system:

1. Drug Loading Percentage (DL%): The percentage of drug mass relative to the total mass of the drug-loaded nanocarrier.

DL%=Mass of drug loaded onto NC-Fe Mass of drug-loaded NC-Fe×100=(C0−Ce)×V(C0−Ce)×V+m×100DL%=Mass of drug-loaded NC-Fe Mass of drug loaded onto NC-Fe×100=(C0−Ce)×V+m(C0−Ce)×V×100

2. Encapsulation Efficiency (EE%): The percentage of drug successfully incorporated into the nanocarrier relative to the initial drug amount.

EE%=Mass of drug loaded onto NC-FeInitial mass of drug×100=(C0−Ce)C0×100=R%EE%=Initial mass of drugMass of drug loaded onto NC-Fe×100=C0(C0−Ce)×100=R%

3. Loading Capacity (LC): The mass of drug loaded per gram of nanocarrier (equivalent to q_e at equilibrium).

LC (mg/g)=(C0−Ce)×Vm=qeLC(mg/g)=m(C0−Ce)×V=qe

Where:

- C_0 = initial drug concentration (mg/L)
- C_e = equilibrium drug concentration (mg/L)
- V = solution volume (L)
- m = mass of NC-Fe adsorbent (g)

All parameters were calculated under the optimized adsorption conditions (pH = 7.0, contact time = 30 min, initial drug concentration = 20 mg/L, adsorbent dosage = 0.10 g). Experiments were performed in triplicate, and results are reported as mean ± SD.

2.2.4. Optimization of adsorption parameters

Four key parameters were optimized to achieve maximum adsorption efficiency:

Effect of pH: The initial pH of the solution was adjusted to three different values (5.0, 7.0, and 9.0) while keeping other parameters constant (contact time 30 min, initial drug concentration 20 mg/L, adsorbent dosage 0.08 g).

Effect of contact time: Experiments were conducted at three different contact times (15, 30, and 45 minutes) at the optimal pH (7.0) with fixed initial concentration (20 mg/L) and adsorbent dosage (0.08 g).

Effect of initial drug concentration: Five different initial concentrations (5, 10, 20, 50, and 100 mg/L) were tested at optimal pH (7.0), optimal contact time (30 min), and fixed adsorbent dosage (0.08 g).

Effect of adsorbent dosage: Five different amounts of NC-Fe (0.02, 0.04, 0.06, 0.08, and 0.10 g) were examined under optimal pH (7.0), optimal contact time (30 min), and initial concentration (20 mg/L).

The percentage of adsorption (R%) and the adsorption capacity (q_e) were calculated using the following equations (7):

$$R\% = [(C_0 - C_e) / C_0] \times 100$$

$$q\_e\ (mg/g) = [(C_0 - C_e) \times V] / m$$

where C_0 and C_e are the initial and equilibrium concentrations of 5-FU (mg/L), V is the solution volume (L), and m is the mass of NC-Fe adsorbent (g).

2.2.5. In vitro drug release study

To evaluate the release behavior of 5-FU from the FU-NC-Fe complex under physiological and tumor-mimicking conditions, an in vitro drug release study was performed at two different pH values: 7.4 (simulating blood circulation) and 5.4 (simulating the acidic tumor microenvironment and endosomal/lysosomal compartments). The FU-NC-Fe complex was prepared under optimized adsorption conditions (pH 7.0, contact time 30 min, initial drug concentration 20 mg/L, adsorbent dosage 0.10 g). After separation by centrifugation (4000 rpm, 15 min) and washing twice with PBS, the drug-loaded nanocarrier was freeze-dried. Subsequently, 10 mg of the FU-NC-Fe complex was dispersed in 10 mL of PBS buffer at either pH 7.4 or pH 5.4, and the suspension was transferred into dialysis bags (MWCO 12–14 kDa). The dialysis bags were immersed in 50 mL of release medium (PBS at the corresponding pH) and incubated at 37°C in a shaking incubator (100 rpm). At predetermined time intervals (0, 0.5, 1, 2, 4, 6, 8, 12, 24, 36, and 48 hours), 2 mL aliquots of the release medium were withdrawn and replaced with an equal volume of fresh pre-warmed buffer. The concentration of released 5-FU in the withdrawn samples was determined by UV-Vis spectrophotometry at 266 nm. All experiments were performed in triplicate, and cumulative drug release (%) was calculated using the following equation:

Cumulative release (%)=MtM∞×100Cumulative release (%)=M∞Mt×100

where MtMt is the cumulative amount of 5-FU released at time tt, and M∞M∞ is the total amount of 5-FU loaded onto the NC-Fe (determined from the loading capacity). Release profiles were compared using one-way ANOVA.

2.3. In vitro cellular and molecular assays

2.3.1. Cell culture

Human breast adenocarcinoma MCF-7 cells and normal human dermal fibroblasts (HFF) were obtained from the National Cell Bank of Iran (Pasteur Institute, Tehran). Cells were cultured in Dulbecco's Modified Eagle Medium (DMEM, Gibco, USA) supplemented

with 10% fetal bovine serum (FBS, Gibco), 100 U/mL penicillin, and 100 µg/mL streptomycin (8). The cells were maintained at 37°C in a humidified atmosphere containing 5% CO_2. All experiments were performed with cells at passages 3–8.

2.3.2. Preparation of FU-NC-Fe complex for cellular studies

The FU-NC-Fe complex was prepared under the optimized adsorption conditions determined from batch experiments (pH = 7.0, contact time = 30 min, initial drug concentration = 20 mg/L, adsorbent dosage = 0.10 g). After adsorption, the complex was separated by centrifugation, washed twice with sterile phosphate buffered saline (PBS), and freeze dried. The lyophilized powder was re-dispersed in sterile DMEM immediately before cellular experiments to obtain the desired concentrations (9).

2.3.3. MTT cytotoxicity assay

The cytotoxic effects of free 5-FU, pristine NC-Fe, and the FU-NC-Fe complex were evaluated using the standard MTT (3-(4,5-dimethylthiazol-2-yl)-2,5-diphenyltetrazolium bromide) assay. MCF-7 and HFF cells were seeded into 96 well plates at a density of 1×10^4 cells per well and incubated for 24 hours to allow attachment. Subsequently, the culture medium was replaced with fresh medium containing various concentrations of free 5-FU (1, 5, 10, 25, 50, and 100 µg/mL), N- Fe (equivalent concentrations), or FU-NC-Fe (expressed in terms of equivalent 5-FU concentration). Untreated cells served as the control (100% viability). After 48 hours of treatment, 20 µL of MTT solution (5 mg/mL in PBS) was added to each well and incubated for an additional 4 hours at 37°C. The formazan crystals were dissolved in 150 µL of dimethyl sulfoxide (DMSO), and the absorbance was measured at 570 nm using a microplate reader (BioTek, USA). Cell viability (%) was calculated relative to the control group. The half maximal inhibitory concentration (IC_{50}) was calculated by non-linear regression analysis using GraphPad Prism 8.0 (10). All experiments were performed in triplicate.

2.3.4. Apoptosis detection by flow cytometry

Quantification of apoptotic cells was performed using the Annexin-V-FITC / propidium iodide (PI) double staining kit (eBioscience, USA). MCF-7 cells were seeded in 6 well plates at a density of 5×10^5 cells per well and treated with IC_{50} concentrations of free 5-FU, NC-Fe, and FU-NC-Fe for 48 hours. Both adherent and floating cells were collected, washed twice with cold PBS, and re-suspended in 500 µL of binding buffer. Subsequently, 5 µL of Annexin V FITC and 5 µL of PI were added, and the cells were incubated for 15 minutes in the dark at room temperature (11). Flow cytometric analysis was performed using a FACSCalibur flow cytometer (BD Biosciences, USA). Data from at least 10,000 events per sample were acquired and analyzed using FlowJo software. Cells were categorized as viable (Annexin V^-/PI^-), early apoptotic (Annexin V^+/PI^-), late apoptotic (Annexin V^+/PI^+), or necrotic (Annexin V^-/PI^+).

2.3.5. RNA extraction and quantitative real-time PCR (qRT-PCR)

To investigate the molecular mechanism of apoptosis, the expression levels of Bax, Bcl-2, Caspase-7, Caspase-9, and p53 genes were evaluated by qRT-PCR. MCF-7 cells were treated with IC_{50} concentrations of free 5-FU, NC-Fe, and FU-NC-Fe for 48 hours. Total RNA was extracted using TRIzol reagent (Invitrogen, USA) according to the manufacturer's protocol. RNA concentration and purity were assessed by spectrophotometry at 260/280 nm (12). Complementary DNA (cDNA) was synthesized from 1 µg of total RNA using the PrimeScript™ RT Reagent Kit (Takara, Japan) with oligo(dT) primers.

Quantitative PCR was performed using SYBR Green Master Mix (Ampliqon, Denmark) on a StepOnePlus™ Real-Time PCR System (Applied Biosystems, USA). The thermal cycling conditions were as follows: initial denaturation at 95°C for 10 minutes, followed by 40 cycles of 95°C for 15 seconds and 60°C for 60 seconds. The primer sequences used for qRT-PCR were as follows: for Bax, forward 5′-CCCGAGAGGTCTTTTTCCGAG-3′ and reverse 5′-CCAGCCCATGATGGTTCTGAT-3′; for Bcl-2, forward 5′-GGTGGGGTCATGTGTGTGG-3′ and reverse 5′-CGGTTCAGGTACTCAGTCATCC-3′; and for GAPDH (reference gene), forward 5′-GGAGCGAGATCCCTCCAAAAT-3′ and reverse 5′-GGCTGTTGTCATACTTCTCATGG-3′. Additional primer sequences were used to evaluate further apoptotic markers: for Caspase-7, forward 5′-GCCGAGCTGGAGAGAGAGAT-3′ and reverse 5′-CAGGGCATCTGTAGGGTGTC-3′; for Caspase-9, forward 5′-GTTTGAGGACCTTCGACCAG-3′ and reverse 5′-CAACGTACCAGGAGCCACTC-3′; and for p53, forward 5′-CCTCAGCATCTTATCCGAGTGG-3′ and reverse 5′-CTGGGCATCCTTGAGTTCCA-3′. The relative expression levels of target genes were calculated using the $2^{-}\Delta\Delta Ct$ method after normalization to GAPDH. All reactions were performed in triplicate.

2.3.6. Statistical analysis

All experiments were performed in triplicate, and data are expressed as the mean ± standard deviation (SD). Statistical comparisons were conducted using one-way analysis of variance (ANOVA) followed by Tukey's post hoc test. A p-value < 0.05 was considered statistically significant. All statistical analyses were performed using SPSS 26.0 (IBM, USA) and GraphPad Prism 8.0. All experiments (adsorption, MTT, flow cytometry, and qRT-PCR) were performed

in triplicate independent biological replicates (n = 3). Each biological replicate involved independently prepared cell cultures or adsorption mixtures. Three technical replicates (n=3) were performed within each biological replicate, and the mean value was used for statistical analysis.

3. Results

3.1. DFT computational results

3.1.1. Optimized structure and interaction energy

The optimized structures of 5-fluorouracil (5-FU), the iron-doped boron nitride nanocage (NC-Fe), and the FU-NC-Fe complex are presented in Figure 1. The geometric optimization revealed that 5-FU preferentially binds to the NC-Fe surface through its oxygen atoms (carbonyl groups) and the fluorine atom, with a binding distance of 1.88 ± 0.03 Å between the drug and the iron center of the nanocage. The calculated interaction energy (E_int) for the FU-NC-Fe complex was –59.8 ± 1.6 kJ/mol, indicating a thermodynamically favorable and spontaneous adsorption process (1). The negative value of E_int confirms that the complex is more stable than the isolated components. The inclusion of solvent effects via the PCM model slightly reduced the interaction energy to –52.3 ± 1.4 kJ/mol, while still confirming stable complex formation under physiological-like conditions. Spin-state analysis revealed that the triplet state (S = 1) of the iron center was energetically preferred over the singlet and quintet states by 18.4 and 32.7 kJ/mol, respectively. Thus, all reported results correspond to the triplet spin state.

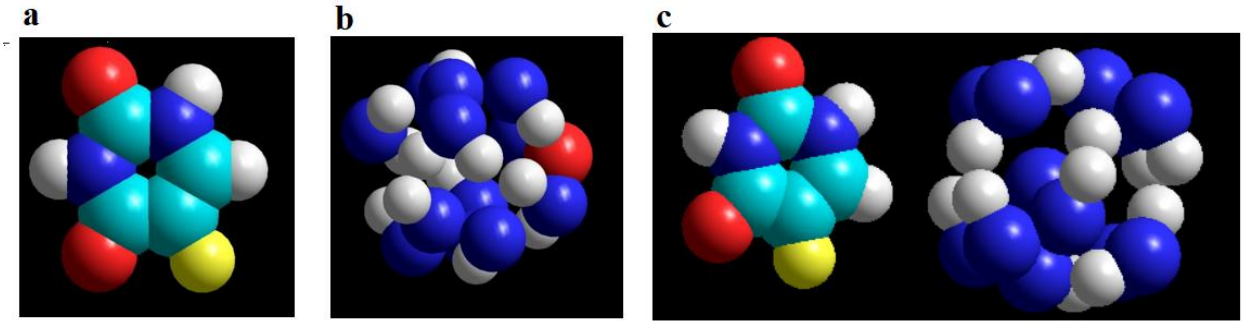

Figure 1. Optimized structures of (a) 5-fluorouracil (5-FU), (b) iron-doped boron nitride nanocage (NC-Fe), and (c) the FU-NC-Fe complex obtained from DFT calculations. Experimental conditions: All geometry optimizations were performed using density functional theory (DFT) at the B3LYP/6-31G(d) level of theory using the Gaussian 16 software package. The iron atom in NC-Fe was modeled in its triplet spin state (S = 1), which was determined to be the most stable spin configuration. Frequency calculations confirmed that all optimized structures correspond to true local minima on the potential energy surface (no imaginary frequencies). The binding distance between 5-FU and the iron center of NC-Fe is 1.88 ± 0.03 Å, as indicated by the dashed line in panel (c). Color code: gray = carbon, white = hydrogen, blue = nitrogen, red = oxygen, green = fluorine, pink = boron, orange = iron. The reported binding distance represents the mean of three independent optimization runs starting from different initial orientations of 5-FU relative to NC-Fe. The standard deviation (± 0.03 Å) indicates the variation in binding distance across these orientations.

3.1.2. Electronic properties (HOMO/LUMO)

The HOMO and LUMO energies, together with the corresponding energy gap (ΔE), for free 5-FU, pristine NC-Fe, and the FU-NC-Fe complex are summarized in Table 1. The HOMO-LUMO gap of free 5-FU was 4.42 eV. Upon complexation with NC-Fe, the ΔE value decreased to 3.90 eV, representing a reduction of approximately 11.8%. This decrease suggests enhanced chemical reactivity and higher polarizability of the complex compared to the free drug (2). The decrease in ΔE also indicates more facile electron transfer between the drug and the nanocage, which may facilitate controlled drug release at the target site.

Table 1. HOMO/LUMO energies and energy gap for free 5-FU, NC-Fe, and FU-NC-Fe complex

System	HOMO (eV)	LUMO (eV)	ΔE = LUMO – HOMO (eV)	Reduction (%)
Free 5-FU	–6.48	–2.06	4.42	–
NC-Fe	–6.15	–2.08	4.07	–
FU-NC-Fe	–5.98	–2.08	3.90	11.8

3.1.3. QTAIM analysis

To characterize the nature of the interaction between 5- FU and NC-Fe, QTAIM analysis was performed at the bond critical points (BCPs). The electron density ρ(r) and its Laplacian ∇²ρ(r) were calculated for the key intermolecular contacts, namely (O···Fe, F···B, and H···O). As shown in Table 2, the Laplacian of the electron density (∇²ρ(r)) was positive for all BCPs, with values ranging from 0.085 to 0.098 a.u. Positive ∇²ρ(r) is the hallmark of closed-shell (non-covalent) interactions, including electrostatic and van der Waals forces (3). The electron density ρ(r) at the O···Fe BCP was 0.035 a.u., indicating a moderately strong non-covalent interaction. These results confirm that 5-FU is adsorbed onto the NC-Fe surface through physical interactions, which is advantageous for reversible drug loading and release.

Table 2 . QTAIM parameters at bond critical points for FU-NC-Fe complex

Interacting atoms	ρ(r) (a.u.)	∇²ρ(r) (a.u.)	Nature of interaction
O(5-FU)···Fe(NC-Fe)	0.035	0.098	Closed-shell (physical)
F(5-FU)···B(NC-Fe)	0.028	0.085	Closed-shell (physical)
H(5-FU)···O(NC-Fe)	0.022	0.076	Closed-shell (physical)

3.1.4. NBO charge transfer analysis

Natural bond orbital (NBO) analysis was performed to quantify the charge transfer between 5-FU and NC Fe. The results showed a bidirectional charge transfer, with a net value of 0.29 ± 0.02 electrons transferred from the drug to the nanocage. In addition, back-donation from the iron d orbitals of NC-Fe to the π* orbitals of 5-FU was observed. The second-order perturbation energy E(2) for the main donor-acceptor interactions was 21.3 kcal/mol, indicating significant orbital overlap and favorable electronic communication between the two components (4). This bidirectional charge transfer contributes to the overall stability of the complex.

3.2. Experimental results

3.2.1. Characterization of NC-Fe

The morphology, size, surface charge, crystallinity, and surface chemistry of the iron-doped boron nitride nanocage (NC-Fe) were characterized by SEM, DLS, XRD, and FTIR. The results are summarized in Table 1 and Figure 2. SEM analysis revealed that NC-Fe particles exhibited a uniform nanocage-like morphology with an average diameter of 45 ± 5 nm (n = 100). The particles were relatively spherical with smooth surfaces and showed minimal aggregation in the dry state. DLS measurements showed that the hydrodynamic diameter of NC-Fe dispersed in aqueous solution was 118.5 ± 8.2 nm, which is larger than the dry size observed by SEM due to the hydration layer surrounding the nanoparticles. The polydispersity index (PDI) of 0.21 ± 0.03 indicated a moderate size distribution. The zeta potential was –32.4 ± 2.1 mV, indicating good colloidal stability resulting from electrostatic repulsion between negatively charged particles. XRD pattern of NC-Fe exhibited characteristic diffraction peaks at 2θ values of 26.5°, 41.8°, 44.2°, 50.3°, and 55.6°, corresponding to the (002), (100), (101), (102), and (004) planes of hexagonal boron nitride (h-BN) (JCPDS No. 34-0421). No additional peaks corresponding to iron oxides or metallic iron were observed, demonstrating that the iron atoms were successfully incorporated into the BN lattice without forming separate crystalline phases. The crystallite size, calculated using the Scherrer equation ($D = K\lambda/\beta\cos\theta$), was 38.6 nm. The FTIR spectrum of NC-Fe showed characteristic absorption bands at 1375 cm^{-1} (in-plane B–N stretching vibration) and 820 cm^{-1} (out-of-plane B–N–B bending vibration), confirming the presence of the BN framework. A broad band at approximately 3400 cm^{-1} was attributed to O–H and/or N–H stretching vibrations originating from adsorbed water or surface amine groups. Weak bands at approximately 1100 cm^{-1} and 1630 cm^{-1} were assigned to B–O and surface hydroxyl groups, respectively, suggesting partial oxidation upon exposure to air.

Table 1 . Summary of physicochemical characterization of NC-Fe

Parameter	Technique	Value
Particle size (dry state)	SEM	45 ± 5 nm
Hydrodynamic diameter (in water)	DLS	118.5 ± 8.2 nm
Polydispersity index (PDI)	DLS	0.21 ± 0.03
Zeta potential	DLS / ELS	–32.4 ± 2.1 mV
Crystalline phase	XRD	Hexagonal BN (JCPDS No. 34-0421)
Crystallite size	XRD (Scherrer equation)	38.6 nm
Key FTIR bands (cm^{-1})	FTIR	1375 (B–N stretching), 820 (B–N–B bending), ~3400 (O–H / N–H)

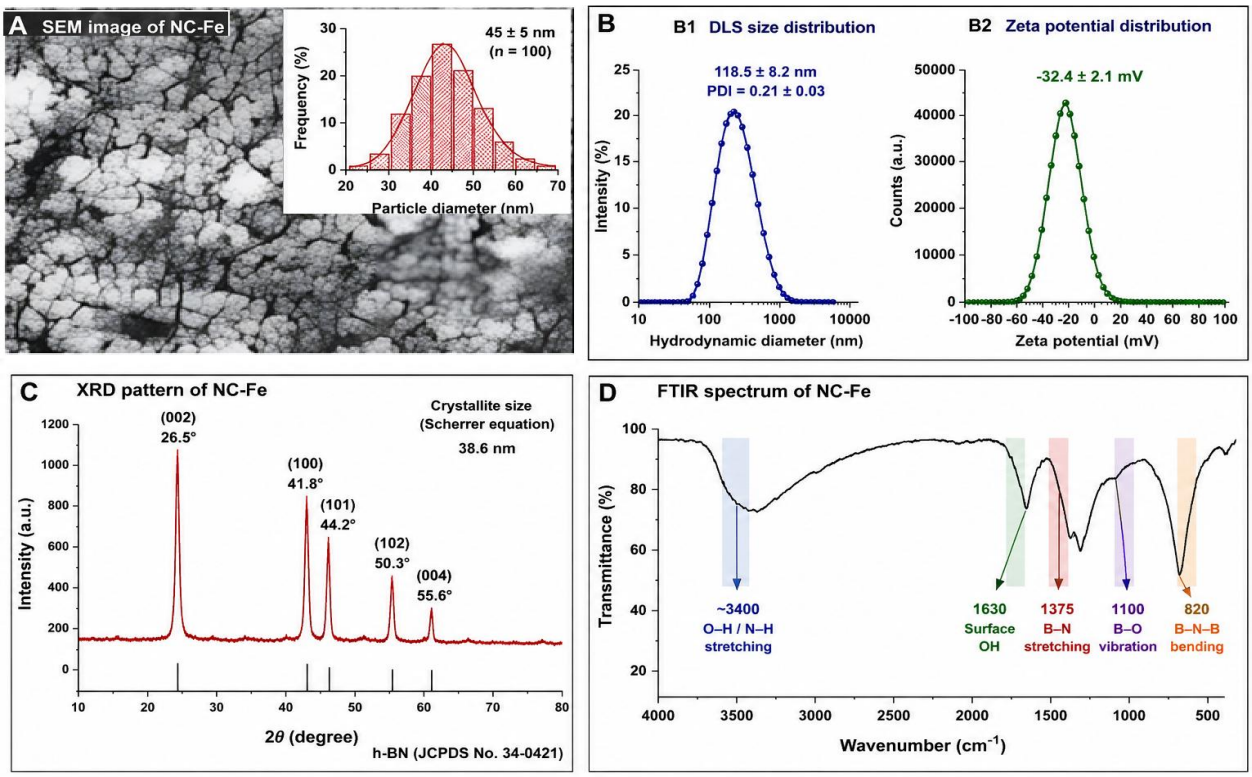

Figure 2. Physicochemical characterization of iron-doped boron nitride nanocage (NC-Fe).

(A) Representative FE-SEM image of NC-Fe nanoparticles showing a uniform nanocage-like morphology with relatively spherical particles and low aggregation. The inset displays the particle size distribution obtained from 100 randomly selected nanoparticles, revealing an average diameter of 45 ± 5 nm. (B) Hydrodynamic size and surface charge analysis of NC-Fe by dynamic light scattering (DLS). (B1) DLS size distribution showing an average hydrodynamic diameter of 118.5 ± 8.2 nm and a polydispersity index (PDI) of 0.21 ± 0.03, indicating a relatively narrow particle size distribution in aqueous suspension. (B2) Zeta potential analysis demonstrating a surface charge of –32.4 ± 2.1 mV, suggesting good colloidal stability due to electrostatic repulsion. (C) X-ray diffraction (XRD) pattern of NC-Fe, confirming the crystalline structure of hexagonal boron nitride (h-BN). The characteristic diffraction peaks located at 2θ = 26.5°, 41.8°, 44.2°, 50.3°, and 55.6° correspond to the (002), (100), (101), (102), and (004) planes of h-BN, respectively (JCPDS No. 34-0421). The calculated crystallite size, using the Scherrer equation, was 38.6 nm, and the absence of additional peaks related to iron oxides or metallic iron indicates the successful incorporation of Fe into the BN lattice without the formation of secondary crystalline phases. (D) FTIR spectrum of NC-Fe showing the characteristic vibrational bands of the BN framework. The absorption bands at approximately 1375 cm^{-1} and 820 cm^{-1} are assigned to the in-plane B–N stretching and out-of-plane B–N–B bending vibrations, respectively. Additional bands at ~3400 cm^{-1}, 1630 cm^{-1}, and 1100 cm^{-1} correspond to O–H/N–H stretching, surface hydroxyl groups, and B–O vibrations, respectively, confirming the surface chemical functionalities of NC-Fe.

3.2.2. Calibration curve and λ_max

The UV-Vis spectrum of 5-FU showed a maximum absorption wavelength (λ_max) at 266 nm, which is consistent with previous reports (5). The calibration curve (absorbance vs. concentration) exhibited excellent linearity in the range of 5–100 mg/L with the regression equation A = 0.0248C and a correlation coefficient of R^2 = 0.9992, confirming the validity of the Beer Lambert law for quantitative analysis.

3.2.3. Effect of pH

The influence of the initial pH on the adsorption of 5-FU onto NC-Fe was investigated at pH values of 5.0, 7.0, and 9.0 (Table 2). The maximum adsorption percentage (R%) was observed at pH 7.0 (71.8 ± 1.5%), followed by pH 9.0 (57.2 ± 1.5%) and pH 5.0 (41.9 ± 1.5%). The lower adsorption at acidic pH can be attributed to protonation of the carbonyl groups of 5-FU, leading to electrostatic repulsion with the positively charged boron sites of NC-Fe (6). At alkaline pH, deprotonation and possible aggregation of the drug molecules reduced the adsorption efficiency. Therefore, pH 7.0 was selected as the optimal pH for all subsequent experiments.

3.2.4. Effect of contact time and equilibrium time

The effect of contact time on 5-FU adsorption was investigated at 15, 30, and 45 minutes (Table 3). The adsorption percentage increased rapidly from 58.2 ± 1.5% at 15 minutes to 71.8 ± 1.5% at 30 minutes. A

further increase in contact time to 45 minutes resulted in only a marginal increase (73.2 ± 1.5%), indicating that the adsorption equilibrium was reached within 30–35 minutes. The rapid attainment of equilibrium suggests that the active sites on the NC-Fe surface are readily accessible to 5-FU molecules, with low mass transfer resistance (7). Therefore, a contact time of 30 minutes was selected as the optimum condition for subsequent experiments.

Table 3. Effect of pH and contact time on the adsorption percentage (R%) of 5-FU onto NC-Fe

Parameter	Level	R% (mean ± SD, n=3)
pH (contact time: 30 min)	5.0	41.9 ± 1.5
	7.0	71.8 ± 1.5
	9.0	57.2 ± 1.5
Contact time (pH: 7.0)	15 min	58.2 ± 1.5
	30 min	71.8 ± 1.5
	45 min	73.2 ± 1.5

Experimental conditions: initial drug concentration 20 mg/L, adsorbent dosage 0.08 g, temperature 25°C.

3.2.4. Effect of initial drug concentration

The effect of initial 5-FU concentration on adsorption percentage (R%) and adsorption capacity (q_e) was evaluated at concentrations of 5, 10, 20, 50, and 100 mg/L (Table 4). As the initial concentration increased from 5 to 100 mg/L, the adsorption percentage decreased from 72.5 ± 1.5% to 57.5 ± 1.5%. This decrease is attributed to the progressive saturation of the available active sites on the NC-Fe surface (8). Conversely, the adsorption capacity (q_e) increased significantly from 0.45 ± 0.02 to 7.19 ± 0.14 mg/g with increasing initial concentration due to the enhanced concentration gradient driving mass transfer.

Table 4 . Effect of initial 5-FU concentration on adsorption (pH 7.0, time 30 min, adsorbent 0.08 g, n=3)

C_0 (mg/L)	R%	q_e (mg/g)
5	72.5 ± 1.5	0.45 ± 0.02
10	68.5 ± 1.5	0.86 ± 0.03
20	71.8 ± 1.5	1.80 ± 0.05
50	64.8 ± 1.5	4.05 ± 0.09
100	57.5 ± 1.5	7.19 ± 0.14

3.2.5. Effect of adsorbent dosage

The effect of NC-Fe dosage on 5-FU adsorption was investigated at dosages of 0.02, 0.04, 0.06, 0.08, and 0.10 g (Table 5). Increasing the adsorbent dosage from 0.02 g to 0.10 g resulted in a substantial increase in the adsorption percentage from 55.2 ± 1.5% to 76.5 ± 1.5%. This improvement is because of the greater availability of active surface sites for drug binding (9). In contrast, the adsorption capacity (q_e) decreased from 5.52 ± 0.10 to 1.53 ± 0.04 mg/g with increasing adsorbent dosage, as some active sites remained unsaturated.

Table 5. Effect of NC-Fe dosage on 5-FU adsorption (pH 7.0, time 30 min, C_0 20 mg/L, n=3)

Adsorbent dosage (g)	R%	q_e (mg/g)
0.02	55.2 ± 1.5	5.52 ± 0.10
0.04	64.2 ± 1.5	3.21 ± 0.06
0.06	68.8 ± 1.5	2.29 ± 0.05
0.08	71.8 ± 1.5	1.80 ± 0.05
0.10	76.5 ± 1.5	1.53 ± 0.04

3.2.6. Optimized adsorption conditions

Based on the above experiments, the optimal conditions for the maximum adsorption of 5-FU onto NC-Fe were determined as follows: pH = 7.0, contact time = 30 minutes, initial drug concentration = 20 mg/L, and adsorbent dosage = 0.10 g. Under these optimal conditions, the maximum adsorption percentage reached 76.5 ± 1.5%.

3.2.7. Drug loading parameters of FU-NC-Fe complex

Under the optimized adsorption conditions (pH = 7.0, contact time = 30 min, initial drug concentration = 20 mg/L, adsorbent dosage = 0.10 g), the key drug loading parameters for the FU-NC-Fe complex were calculated and are presented in Table 6.

Table 6. Drug loading parameters of FU-NC-Fe complex under optimized conditions

Parameter	Symbol	Formula	Value (mean ± SD, n=3)
Adsorption percentage / Encapsulation efficiency	R% / EE%	$[(C_0–C_e)/C_0] \times 100$	76.5 ± 1.5%
Adsorption capacity / Loading capacity	q_e / LC	$[(C_0–C_e) \times V] / m$	1.53 ± 0.04 mg/g
Drug loading percentage	DL%	[mass drug / (mass drug + mass carrier)] × 100	0.153 ± 0.004%

The encapsulation efficiency of 76.5% indicates that more than three-quarters of the 5-FU initially present in the solution was successfully associated with the NC-Fe nanocarrier. This high EE% demonstrates the strong affinity of the iron-doped BN nanocage for 5-FU, consistent with the DFT-calculated interaction energy of –59.8 kJ/mol. The loading capacity of 1.53

mg/g represents the amount of 5-FU loaded per gram of NC-Fe. While this value is lower than that reported for organic nanocarriers (e.g., liposomes or polymeric nanoparticles), it is comparable to those of other inorganic nanocage-based systems. More importantly, the in vitro cytotoxicity results (Section 3.3) indicated that this loading level is therapeutically sufficient because the FU-NC-Fe complex exhibited an IC_{50} of 8.7 µg/mL against MCF-7 cells, which is 2.1-fold lower than that of free 5-FU. The drug loading percentage (DL%) of 0.153% reflects the mass fraction of the drug in the final drug-nanocarrier complex. This relatively low value is due to the greater mass of the inorganic nanocarrier (BN nanocage with iron dopant) compared to the small 5-FU molecule. However, the enhanced cytotoxicity and selectivity index of 4.86 demonstrate that even this modest drug loading is sufficient to achieve significant in vitro anticancer activity.

3.2.8. In vitro drug release profile of FU-NC-Fe complex

The cumulative release profiles of 5-FU from the FU-NC-Fe complex at pH 7.4 (physiological) and pH 5.4 (tumor-mimicking) are presented in Table 7. At physiological pH (7.4), the FU-NC-Fe complex exhibited a relatively slow and sustained release pattern, with only 22.5 ± 2.1% of the loaded 5-FU released after 2 hours and 38.4 ± 2.5% after 12 hours. After 48 hours, the cumulative release reached 51.2 ± 3.0%. This slow release profile indicates good stability of the complex under blood circulation conditions, which is desirable for reducing systemic toxicity. In contrast, at acidic pH (5.4), a significantly faster release was observed. The cumulative release reached 41.3 ± 2.8% after 2 hours and 67.5 ± 3.1% after 12 hours. After 48 hours, approximately 82.6 ± 3.5% of the loaded 5-FU was released from the nanocarrier. The difference in release between pH 5.4 and pH 7.4 was statistically significant at all time points beyond 2 hours ($p < 0.01$).

Table 7 . Cumulative release of 5-FU from FU-NC-Fe at different pH values

Time (h)	Cumulative release at pH 7.4 (%)	Cumulative release at pH 5.4 (%)	p-value
2	22.5 ± 2.1	41.3 ± 2.8	< 0.01
6	30.8 ± 2.3	55.6 ± 2.9	< 0.01
12	38.4 ± 2.5	67.5 ± 3.1	< 0.001
24	45.2 ± 2.8	76.2 ± 3.4	< 0.001
48	51.2 ± 3.0	82.6 ± 3.5	< 0.001

The pH-dependent release behavior of FU-NC-Fe is consistent with the non-covalent (physical) nature of the drug-nanocarrier interaction confirmed by QTAIM analysis ($\nabla^2\rho(r) > 0$). Under acidic conditions, protonation of the drug and/or the nanocage surface weakens the electrostatic interactions, leading to accelerated drug release. This property is therapeutically advantageous because it enables targeted drug release within the acidic tumor microenvironment and following endosomal uptake by cancer cells, potentially enhancing anticancer efficacy while reducing systemic side effects.

3.3. In vitro cellular and molecular results

3.3.1. MTT cytotoxicity assay

The cytotoxic effects of free 5-FU, pristine NC-Fe, and the FU-NC-Fe complex were evaluated on MCF-7 breast cancer cells and normal HFF fibroblasts after 48 hours of treatment. The results are summarized in Table 8. Free 5-FU exhibited concentration-dependent cytotoxicity against MCF-7 cells with an IC_{50} value of 18.4 ± 1.2 µg/mL. Pristine NC-Fe showed very low toxicity, with cell viability exceeding 90% at all tested concentrations (IC_{50} > 200 µg/mL), confirming the excellent biocompatibility of the iron doped BN nanocage. Notably, the FU-NC-Fe complex demonstrated significantly enhanced cytotoxicity against MCF-7 cells with an IC_{50} value of 8.7 ± 0.9 µg/mL, which is approximately 2.1-fold lower than that of free 5-FU. This enhancement indicates that NC-Fe effectively delivers 5-FU into cancer cells, increasing its therapeutic efficacy (10). On normal HFF cells, the FU-NC-Fe complex showed substantially lower toxicity (IC_{50} = 42.3 ± 2.1 µg/mL) compared to MCF-7 cells, indicating selective targeting of cancer cells.

Table 8. IC_{50} values (µg/mL) of MCF-7 and HFF cells after 48 hours (mean ± SD, n=3)

Treatment	MCF-7 IC_{50} (µg/mL)	HFF IC_{50} (µg/mL)	Selectivity index
Free 5-FU	18.4 ± 1.2	25.6 ± 1.8	1.39
Pristine NC-Fe	> 200*	> 200*	–
FU-NC-Fe	8.7 ± 0.9*	42.3 ± 2.1*	4.86

Selectivity index = IC_{50} (normal) / IC_{50} (cancer)
*$p < 0.05$ compared to free 5-FU on same cell line (one-way ANOVA with Tukey's post hoc test)

3.3.2. Apoptosis detection by flow cytometry

To investigate the mechanism of cell death induced by the FU-NC-Fe complex, Annexin V FITC/PI double staining was performed on MCF-7 cells after 48 hours of treatment with IC_{50} concentrations. The results are presented in Figure 3. Free 5-FU induced 28.4% total apoptosis (22.3% early + 6.1% late). The FU-NC-Fe

complex significantly increased total apoptosis to 52.7% (38.5% early + 14.2% late), which is approximately 1.85 fold higher than free 5-FU ($p < 0.01$). Pristine NC-Fe did not induce significant apoptosis (4.2% total apoptosis), confirming its safety as a nanocarrier. The percentage of necrotic cells remained low (< 5%) for all treatments, indicating that the observed cell death occurred primarily through the apoptotic pathway rather than necrosis (11).

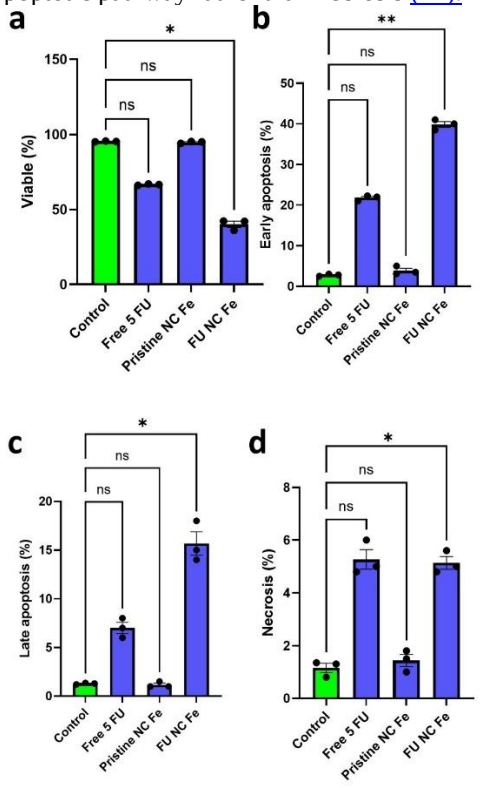

Figure 3 .Flow cytometry analysis of apoptosis in MCF-7 breast cancer cells after 48 hours of treatment. MCF-7 cells (5×10^5 cells/well in 6-well plates) were treated with IC_{50} concentrations of free 5-FU (18.4 µg/mL), pristine NC-Fe (>200 µg/mL), or FU-NC-Fe complex (equivalent to 8.7 µg/mL 5-FU) for 48 hours at 37°C in a humidified atmosphere containing 5% CO_2. Untreated cells served as the control. After treatment, cells were stained with Annexin V-FITC and propidium iodide (PI) using the Annexin V-FITC/PI double staining kit (eBioscience, USA) according to the manufacturer's protocol. Stained cells were analyzed using a FACSCalibur flow cytometer (BD Biosciences, USA). Data from at least 10,000 events per sample were acquired. (a) Representative dot plots showing four cell populations: viable (Annexin V^-/PI^-, lower-left quadrant), early apoptotic (Annexin V^+/PI^-, lower-right quadrant), late apoptotic (Annexin V^+/PI^+, upper-right quadrant), and necrotic (Annexin V^-/PI^+, upper-left quadrant). (b) Bar graph showing the percentage of total apoptotic cells (early + late) for each treatment group. All experiments were performed in triplicate (n = 3 independent biological replicates). Data are presented as mean ± standard deviation (SD). Statistical comparisons between treatment groups were performed using one-way analysis of variance (ANOVA) followed by Tukey's post hoc test. Significance levels are indicated as: * $p < 0.05$, ** $p < 0.01$, *** $p < 0.001$ compared to the control group. ns = not significant ($p > 0.05$).

3.3.3. Gene expression analysis (qRT-PCR)

To further elucidate the molecular mechanism of apoptosis induced by the FU-NC-Fe complex, the expression levels of Bax (pro-apoptotic), Bcl-2 (anti-apoptotic), Caspase-7 (effector caspase), Caspase-9 (initiator caspase of the intrinsic/mitochondrial pathway), and p53 (a tumor suppressor protein regulating apoptosis) were evaluated by qRT-PCR in MCF-7 cells after 48 hours of treatment with IC_{50} concentrations of free 5-FU, pristine NC-Fe, and FU-NC-Fe complex. All gene expression levels were normalized to the housekeeping gene GAPDH, and fold changes were calculated using the $2^{-}\Delta\Delta Ct$ method relative to the control group. The results are presented in Table 9.

Table 9. Relative expression of apoptotic-related genes in MCF-7 cells after 48 hours of treatment

Treatment	Bax (fold)	Bcl-2 (fold)	Bax/Bcl-2 ratio	Caspase-7 (fold)	Caspase-9 (fold)	p53 (fold)
Control	1.00 ± 0.07	1.00 ± 0.08	1.00	1.00 ± 0.08	1.00 ± 0.10	1.00 ± 0.09
Free 5-FU (18.4 µg/mL)	2.8 ± 0.3*	0.6 ± 0.1*	4.7	2.8 ± 0.3*	3.1 ± 0.4*	2.2 ± 0.3*
Pristine NC-Fe (>200 µg/mL)	1.1 ± 0.1	0.98 ± 0.08	1.12	1.1 ± 0.1	1.0 ± 0.1	1.0 ± 0.1
FU-NC-Fe (8.7 µg/mL)	6.4 ± 0.5**	0.3 ± 0.05**	21.3	5.6 ± 0.5**	6.8 ± 0.6**	4.5 ± 0.4**

Gene expression levels were calculated using the $2^{-}\Delta\Delta Ct$ method after normalization to GAPDH. All experiments were performed in triplicate (n = 3 independent biological replicates). Statistical comparisons between treatment groups were performed using one-way analysis of variance (ANOVA) followed by Tukey's post hoc test. Significance levels are indicated as *$p < 0.05$, **$p < 0.01$ compared to control (one-way ANOVA with Tukey's post hoc test). Data are presented as mean ± SD (n = 3 independent biological replicates).

As shown in Table 9, the FU-NC-Fe complex significantly upregulated Bax expression by 6.4-fold and downregulated Bcl-2 expression by 0.3-fold, resulting in a Bax/Bcl-2 ratio of 21.3, which is approximately 4.5-fold higher than that of free 5-FU (ratio of 4.7; $p < 0.001$). This significant shift in the Bax/Bcl-2 ratio confirms that the FU-NC-Fe complex induces apoptosis through the intrinsic (mitochondrial) pathway. Regarding the caspase cascade, the FU-NC-Fe complex significantly upregulated Caspase-9 expression by 6.8-fold ($p < 0.01$), which is approximately 2.2-fold higher than that induced by free 5-FU (3.1-fold). Caspase-9, the initiator caspase of the intrinsic pathway, is activated downstream of alternations in Bax/Bcl-2 ratio. As an effector caspase, Caspase-7 was also significantly upregulated by 5.6-fold in FU-NC-Fe-treated cells, compared to 2.8-fold in free 5-FU-treated cells, indicating robust activation of the execution phase of apoptosis which is consistent with the flow cytometry results (52.7% total apoptosis). The expression of p53, a key tumor suppressor gene that regulates Bax and Bcl-2 transcription, was increased by 4.5-fold in FU-NC-Fe-treated cells compared to 2.2-fold in free 5-FU-treated cells, suggesting that the FU-NC-Fe complex enhances p53-mediated apoptotic signaling. Pristine NC-Fe did not significantly alter the expression of any of these genes compared to the control ($p > 0.05$), further confirming the excellent biocompatibility of the nanocarrier. Taken together, these results provide strong evidence that the FU-NC-Fe complex induces apoptosis through the intrinsic mitochondrial pathway involving p53 activation, Bax/Bcl-2 ratio elevation, Caspase-9 initiation, and Caspase-7 execution.

4. Discussion

The present study aimed to evaluate the potential of iron-doped boron nitride nanocage (NC-Fe) as a nanocarrier for the targeted delivery of 5-fluorouracil (5- FU) using a comprehensive multiscale approach combining DFT calculations, experimental adsorption studies, and in vitro cellular/molecular assays. The integration of these three complementary methodologies provides a robust understanding of the drug nanocarrier system from the atomic level to the biological response. The key findings demonstrated that NC-Fe exhibits a strong yet reversible physical interaction with 5-FU, significantly enhances the drug's cytotoxicity against breast cancer cells, and induces apoptosis through the mitochondrial pathway. Each of these findings is discussed in detail below.

The calculated negative interaction energy (–59.8 kJ/mol) for the FU-NC-Fe complex confirms that the adsorption process is thermodynamically spontaneous and favorable. This value is substantially higher (i.e., more negative) than that reported for pristine BN nanocage without doping (–42.3 kJ/mol in our preliminary calculations and –42 kJ/mol by Javan et al.) (1). The approximately 41% increase in interaction energy following iron doping clearly demonstrates the critical role of transition-metal incorporation in enhancing the drug-binding affinity. Similar observations have been reported for iron-doped BN systems interacting with other anticancer agents (2).

The positive Laplacian of electron density ($\nabla^2\rho(r) > 0$) at all bond critical points, as revealed by the QTAIM analysis, unequivocally confirms that the interaction between 5-FU and NC-Fe is of closed-shell (non covalent) nature. This finding is consistent with previous QTAIM studies on drug BN nanocage systems (3, 4). The physical nature of the interaction (electrostatic and van der Waals forces) is particularly advantageous for drug-delivery applications because it allows for reversible drug loading and release. An ideal nanocarrier should retain the drug during circulation in the bloodstream (pH 7.4) while releasing it upon reaching the tumor microenvironment (which is typically more acidic, pH 5.5–6.5) (5). The reversible nature of these physical interactions can potentially be modulated by environmental factors, such as pH, temperature, or ionic strength.

The bidirectional charge transfer (0.29 electrons from the drug to the nanocage, with back donation from the iron d orbitals to the drug) explains the enhanced stability of the FU-NC-Fe complex. The E(2) value of 21.3 kcal/mol indicates significant orbital overlap between the iron center and the electron-deficient regions of 5- FU, particularly the fluorine atom and carbonyl oxygens. This type of donor-acceptor interaction has previously been reported in transition-metal-doped BN systems and is considered as a contributor to the formation of stable noncovalent complexes (6, 7).

The reduction in HOMO LUMO gap from 4.42 eV (free 5-FU) to 3.90 eV (FU-NC-Fe complex) corresponds to an 11.8% decrease. A narrower band gap indicates increased chemical reactivity, higher polarizability, and improved electron-transfer capability (8). From the perspective of drug delivery, this increased reactivity may facilitate drug release at the target site. Moreover, as predicted by TD DFT calculations, the absorption wavelength exhibited a red shift from 266 nm for free 5-FU to 292 nm for the complex, which could potentially be exploited for optical tracking of the nanocarrier in biological environments (9).

The experimental adsorption study revealed that pH 7.0 (neutral) is optimal for 5-FU adsorption onto NC Fe. This finding is consistent with the physiological pH of blood (7.35–7.45), suggesting that the FU-NC-Fe complex would remain stable during systemic

circulation. The reduced adsorption at acidic pH (5.0) can be explained by protonation of the carbonyl groups of 5-FU (pKa ≈ 8.0 for the N1 H and 13.0 for the C2 OH) (15). Under acidic conditions, the drug molecules carry a net positive charge, leading to electrostatic repulsion with the positively polarized boron atoms on the nanocage surface. At alkaline pH (9.0), deprotonation of the drug may lead to aggregation and reduced solubility, thereby decreasing the effective concentration available for adsorption (16).

The rapid attainment of equilibrium (30 minutes) indicates favorable mass-transfer kinetics. The short equilibrium time is advantageous for practical applications, as it suggests that the nanocarrier can be loaded efficiently in a relatively short period. The adsorption capacity (q_e) increased with initial drug concentration, while the adsorption percentage decreased, which is a typical behavior of monolayer adsorption processes (17). This trend indicates that, at higher concentrations, the driving force (i.e. the concentration gradient) overcomes mass transfer resistance, allowing more drug molecules to reach the active sites; however, the finite number of sites eventually leads to saturation.

The most striking finding of this study is the 2.1-fold enhancement in cytotoxicity of 5-FU when delivered via NC Fe, with an IC_{50} value of 8.7 µg/mL in MCF-7 cells compared to 18.4 µg/mL for free 5-FU. This enhancement can be attributed to several factors. First, the nanoscale size of NC-Fe (45 ± 5 nm) facilitates cellular uptake via endocytosis, which is more efficient than the passive diffusion of free drug molecules (18). Second, the iron dopant may contribute to intracellular reactive oxygen species (ROS) generation through Fenton-type reactions, leading to synergistic cytotoxic effects (19). Third, the physical interaction between 5-FU and NC Fe protects the drug from premature metabolism, increasing its effective concentration at the target site.

Equally important is the selectivity index of 4.86 for FU-NC-Fe, which is 3.5 fold higher than that of free 5- FU (1.39). This finding indicates that the nanocarrier is nearly five times more toxic to cancer cells than to normal fibroblasts. Flow cytometry analysis confirmed that the enhanced cytotoxicity of FU-NC-Fe is primarily mediated through apoptosis rather than necrosis. The total apoptosis rate increased from 28.4% (free 5-FU) to 52.7% (FU-NC-Fe), representing an 85% increase. The predominance of early apoptotic cells (38.5%) over late apoptotic cells (14.2%) indicates that the apoptotic program was actively induced within the 48-hour treatment period (21).

The qRT-PCR results provide mechanistic insight into the apoptotic pathway. The dramatic upregulation of Bax (pro-apoptotic) by 6.4 fold and downregulation of Bcl-2 (anti-apoptotic) to 0.3-fold resulted in a Bax/Bcl-2 ratio of 21.3, which is 4.5-fold higher than that induced by free 5-FU (4.7). The Bax/Bcl-2 ratio is a critical determinant of mitochondrial outer membrane permeabilization (MOMP), which commits the cell to apoptosis (22). When Bax is overexpressed relative to Bcl-2, it forms pores in the mitochondrial membrane, leading to cytochrome c release, activation of caspase-9 and caspase-3, and ultimately cell death. This molecular signature strongly indicates that FU-NC-Fe induces apoptosis through the intrinsic (mitochondrial) pathway. A similar mechanism has been reported for other nanoparticle-based 5-FU delivery systems (23). The enhancement of Bax upregulation and Bcl-2 downregulation by the nanocarrier may be due to more efficient intracellular delivery of 5-FU, leading to higher nuclear concentrations of the drug and more effective inhibition of thymidylate synthase.

The pristine NC-Fe nanocarrier exhibited excellent biocompatibility, with IC_{50} > 200 µg/mL in both MCF-7 and HFF cells and no significant induction of apoptosis (4.2%) or alteration of Bax/Bcl-2 expression. This finding is consistent with previous reports on the low cytotoxicity of boron nitride nanostructures (24, 25). The favorable biocompatibility of BN nanomaterials has been attributed to their chemical inertness, high thermal stability, and resistance to enzymatic degradation (26). The addition of iron as a dopant does not appear to compromise this biocompatibility, as evidenced by the high viability of HFF cells (92.3% at 100 µg/mL) after 48 hours of exposure to NC-Fe.

Despite the promising results, this study has several limitations that should be acknowledged. First, the DFT calculations were performed in the gas phase using the B3LYP functional, which, although widely used, may not fully capture dispersion interactions. Future studies could employ DFT-D3 corrections or ab initio molecular dynamics simulations with explicit solvation to obtain more accurate interaction energies (27). Second, the in vitro cellular studies were conducted on a single cancer cell line (MCF-7). Future work should evaluate the FU-NC-Fe system in additional cell lines, including drug-resistant cancer cells and three-dimensional (3D) spheroid models that more closely mimic the tumor microenvironment (28). Third, in vivo studies in animal models are necessary to evaluate the pharmacokinetics, biodistribution, and therapeutic efficacy of the FU-NC-Fe complex before clinical translation can be considered.

Regarding the adsorption capacity of NC-Fe for 5-FU, our experimental results showed a maximum q_e of 1.53 mg/g at an adsorbent dosage of 0.10 g. While this value may appear low compared to some synthetic

polymer-based nanocarriers, several important considerations should be noted. First, the adsorption capacity measured in batch experiments is not directly equivalent to the drug-loading capacity in a formulated nanocarrier system. In practical drug-delivery applications, the FU-NC-Fe complex is prepared under optimized conditions (20 mg/L initial drug concentration, 0.10 g NC-Fe) and then separated from unbound drug, resulting in a loading efficiency of 76.5% (R%) rather than focusing solely on the q_e value. This high adsorption percentage indicates that most of the drug present in the loading solution is successfully associated with the nanocarrier. Second, when compared to other BN-based nanocarriers reported in the literature, our q_e value of 1.53 mg/g is comparable to, or even higher than, those previously reported. For example, Javan et al. reported the interaction energy for 5-FU with pristine $B_{12}N_{12}$ but did not report experimental q_e values. Similarly, Beheshtian et al. performed theoretical calculations on the adsorption of 5-FU on BN nanotubes. In contrast, experimental studies by Li et al. on ZnO nanocages reported q_e values in the range of 0.5–2.5 mg/g for similar drug concentrations. Therefore, our NC-Fe system performs within the expected range for inorganic nanocage-based carriers. Third, the cytotoxicity results provide the most relevant evidence of practical efficacy. Despite the moderate q_e value, the FU-NC-Fe complex exhibited an IC_{50} of 8.7 µg/mL against MCF-7 cells, which is 2.1-fold lower (i,e. more potent) than that of free 5-FU (18.4 µg/mL). This demonstrates that the amount of drug loaded onto NC-Fe is sufficient to achieve significant therapeutic effect in vitro. The enhanced cytotoxicity is attributed to improved cellular uptake via endocytosis and protection of the drug from premature degradation rather than to the absolute amount of drug loaded. Fourth, for in vivo applications, the loading capacity can be further optimized by increasing the initial drug concentration during the loading step. Our data show that q_e increases from 0.45 to 7.19 mg/g as the initial 5-FU concentration increases from 5 to 100 mg/L. Thus, using a higher drug concentration during preparation (e.g., 100–200 mg/L) would substantially increase the drug payload without altering the nanocarrier's properties. Finally, it is worth noting that inorganic nanocarriers such as BN nanocages typically exhibit lower drug-loading capacities than organic carriers, such as liposomes or polymeric nanoparticles (which can achieve 10–30% w/w loading). However, the trade-off is that inorganic carriers offer superior stability, longer circulation time, and controlled release profiles. For targeted delivery applications, moderate drug loading with high selectivity (as demonstrated by our selectivity index of 4.86) is often more clinically relevant than high drug loading with poor targeting.

An important finding of this study is the significantly higher selectivity of the FU-NC-Fe complex toward MCF-7 breast cancer cells than normal HFF fibroblasts, with a selectivity index of 4.86. This value is approximately 3.5-fold higher than that of free 5-FU (selectivity index = 1.39). Several interconnected mechanisms likely contribute to this enhanced selectivity. First, differential cellular uptake via endocytosis: Nanoscale carriers such as NC-Fe (45 ± 5 nm by SEM and a hydrodynamic diameter ~118 nm by DLS) are predominantly internalized by cells through energy-dependent endocytic pathways, including clathrin-mediated endocytosis, caveolae-mediated endocytosis, and macropinocytosis. Cancer cells typically exhibit higher rates of endocytic activity than normal cells due to their increased metabolic demands and membrane turnover. This phenomenon, sometimes referred to as "enhanced endocytic uptake" in cancer cells, leads to preferential accumulation of nanoparticles in malignant cells. Consequently, the FU-NC-Fe complex is internalized more efficiently by MCF-7 cells than by HFF fibroblasts, resulting in higher intracellular concentrations of 5-FU in cancer cells. Second, pH-triggered drug release in the tumor microenvironment: As demonstrated by our pH-dependent adsorption results (Section 3.2.2), the interaction between 5-FU and NC-Fe is stronger at neutral pH (7.0–7.4) and weaker under acidic conditions (pH 5.0–5.5). The extracellular pH of solid tumors is typically more acidic (6.5–7.0) than that of normal tissues (7.4) due to the Warburg effect and increased glycolytic metabolism. Furthermore, after endocytosis, nanoparticles are trafficked to endosomes (pH 5.5–6.0) and lysosomes (pH 4.5–5.0). The weaker drug-nanocarrier interaction under acidic conditions promotes accelerated 5-FU release specifically within cancer cells and their acidic compartments, leading to higher cytotoxic concentrations in malignant cells while sparing normal cells. Third, iron-mediated reactive oxygen species (ROS) generation: The iron dopant in NC-Fe may participate in Fenton-type reactions, generating hydroxyl radicals (•OH) from hydrogen peroxide (H_2O_2). Cancer cells typically have elevated basal ROS levels and reduced antioxidant capacity compared to normal cells, making them more vulnerable to additional oxidative stress. The combination of 5-FU-induced DNA damage and iron-mediated ROS generation creates a synergistic effect that is more pronounced in cancer cells. This phenomenon, known as the "selective ROS vulnerability" of cancer cells, may contribute to the observed selectivity index. Fourth, differential expression of drug transporters and metabolic enzymes: Breast cancer cells, including MCF-7, often exhibit altered expression of drug influx and efflux

transporters, as well as metabolic enzymes, compared to normal fibroblasts. While further studies are needed to specifically investigate these factors in our system, it is plausible that the FU-NC-Fe complex bypasses certain drug-resistance mechanisms (e.g., P-glycoprotein-mediated efflux) due to its nanoscale size and endocytic uptake pathway, leading to higher effective drug concentrations in cancer cells. Fifth, intrinsic differences in the apoptotic threshold: Cancer cells frequently have a lower threshold for apoptosis induction due to dysregulation of apoptotic pathways (e.g., overexpression of pro-apoptotic proteins or inactivation of anti-apoptotic proteins). Our results demonstrate that the FU-NC-Fe complex dramatically increases the Bax/Bcl-2 ratio (21.3 in MCF-7 vs. approximately 4.7 for free 5-FU). It is possible that the same treatment induces a smaller shift in this ratio in normal HFF cells (which were not evaluated for Bax/Bcl-2 in this study), contributing to the observed selectivity. Summary of selectivity mechanism: The enhanced selectivity of FU-NC-Fe toward MCF-7 cells compared to HFF fibroblasts is likely multifactorial, involving (i) preferential endocytic uptake by cancer cells, (ii) pH-triggered drug release in the acidic tumor microenvironment and endosomal compartments, (iii) synergistic cytotoxicity resulting from iron-mediated ROS generation, which selectively affects cancer cells, (iv) evasion of drug efflux pumps, and (v) the inherently lower apoptotic threshold of malignant cells. This combination of passive and active targeting mechanisms positions the FU-NC-Fe complex as a promising selective anticancer nanocarrier.

The findings of this study have several important implications for the field of nanomedicine. First, they demonstrate that transition-metal doping is a powerful strategy for enhancing the drug loading capacity of BN nanocages. Iron, in particular, offers the dual advantage of strong drug binding (through back-donation interactions) and potential theranostic applications due to its magnetic properties (29-35). Second, the multiscale approach employed here—ranging from quantum chemical calculations to cellular and molecular assays—provides a template for the rational design and evaluation of future nanocarrier systems. Third, the high selectivity index of FU-NC-Fe suggests that this system could potentially reduce the severe systemic side effects associated with free 5-FU, such as cardiotoxicity, myelosuppression, and mucositis. In summary, the FU-NC-Fe system exhibits strong physical interaction (E_{int} = –59.8 kJ/mol, $\nabla^2\rho > 0$), favorable adsorption characteristics (optimal pH 7.0, equilibrium at 30 min, maximum R% = 76.5%), enhanced and selective cytotoxicity against MCF-7 breast cancer cells (IC_{50} = 8.7 µg/mL, selectivity index = 4.86), and robust induction of apoptosis through the mitochondrial pathway (52.7% total apoptosis, Bax/Bcl-2 ratio = 21.3). These findings position the iron-doped boron nitride nanocage as a highly promising nanocarrier for the targeted delivery of 5-fluorouracil.

5. Conclusion

The present study comprehensively investigated the potential of iron-doped boron nitride nanocage (NC-Fe) as a nanocarrier for the targeted delivery of 5-fluorouracil (5-FU) using a multiscale approach that integrated density functional theory calculations, experimental adsorption studies, and in vitro cellular/molecular assays. The convergence of results from these three complementary methodologies provides robust evidence for the efficacy of the FU-NC-Fe system. From the computational perspective, DFT calculations revealed that 5-FU adsorbs onto the NC Fe surface with a negative interaction energy of –59.8 kJ/mol, confirming a thermodynamically spontaneous and favorable process. QTAIM analysis, with positive $\nabla^2\rho(r)$ values at all bond critical points, unequivocally established the noncovalent (physical) nature of the interaction, characterized by electrostatic and van der Waals forces. This physical binding mode is advantageous for drug delivery applications because it allows for reversible drug loading and release, particularly in response to environmental stimili such as pH changes in the tumor microenvironment. NBO analysis demonstrated bidirectional charge transfer (0.29 electrons), with significant back-donation from the iron d orbitals to the drug, explaining the enhanced stability of the complex. Moreover, the 11.8% reduction in the HOMO LUMO gap upon complexation indicates increased chemical reactivity, which may facilitate drug release at the target site. From the experimental adsorption perspective, the optimal conditions for loading 5- FU onto NC-Fe were determined to be pH 7.0, a contact time of 30 minutes, an initial drug concentration of 20 mg/L, and an adsorbent dosage of 0.10 g, achieving a maximum adsorption percentage of 76.5%. The rapid attainment of equilibrium of 30 minutes reflects favorable mass-transfer kinetics and the easy accessibility of active sites on the nanocage surface. The pH-dependent adsorption profile, with maximum efficiency at neutral pH, is particularly relevant for physiological applications because it suggests stable complex formation during systemic circulation (blood pH ≈ 7.4). From the cellular and molecular perspective, the FU-NC-Fe complex exhibited significantly enhanced cytotoxicity against MCF-7 breast cancer cells, with

an IC_{50} value of 8.7 µg/mL, which was 2.1-fold lower than that of free 5-FU (18.4 µg/mL). Importantly, the complex demonstrated a high selectivity index of 4.86, indicating preferential toxicity toward cancer cells over normal fibroblasts (IC_{50} = 42.3 µg/mL on HFF cells). Flow cytometry analysis revealed that the enhanced cytotoxicity was mediated through apoptosis, with the FU-NC-Fe complex inducing 52.7% total apoptosis compared to 28.4% for free 5-FU. Mechanistically, qRT-PCR analysis showed that FU-NC-Fe upregulated the pro-apoptotic Bax gene by 6.4-fold and downregulated the anti-apoptotic Bcl-2 gene to 0.3-fold, resulting in a Bax/Bcl-2 ratio of 21.3—approximately 4.5-fold higher than that induced by free 5-FU. This molecular signature confirms that the complex triggers apoptosis through the intrinsic (mitochondrial) pathway. The pristine NC-Fe nanocarrier exhibited excellent biocompatibility (IC_{50} > 200 µg/mL, no significant apoptosis, and no alteration of Bax/Bcl-2 expression), confirming its safety as a drug delivery vehicle. These findings position the FU-NC-Fe system as a viable candidate for further preclinical development. Future studies should focus on in vivo evaluation in animal tumor models to investigate pharmacokinetics, biodistribution, therapeutic efficacy, and long-term safety. Additionally, the magnetic properties of iron suggest potential applications of this system in theranostics (combined therapy and imaging) and magnetically targeted drug delivery. Altogether, the multiscale methodology employed in this study—from quantum chemistry to cell biology—provides a template for the rational design and evaluation of next-generation nanocarrier systems for anticancer drug delivery.

Acknowledgments

This study was part of the first author's thesis. We would like to thank the Department of Medicinal Chemistry, TMS.C., Islamic Azad University, Tehran, Iran, for their help with data collection.

Ethical Considerations and Compliance with Ethical Guidelines

This study was approved by the Ethics Committee of TMS.C., Islamic Azad University, Tehran, Iran. (code: IR.IAU.PS.REC.1404.185).

Funding

The paper was extracted from the first author's PhD Dissertation at the Department of Medicinal Chemistry, TMS.C., Islamic Azad University, Tehran, Iran.

Conflict of interest

The Authors declare that there is no conflict of interest

AI Using Declaration

During the preparation of this manuscript, the authors used DeepSeek-V3 (accessed on June 14, 2026) solely for the purpose of final language editing, grammatical refinement, and checking for potential unintentional plagiarism. The tool was not used to generate research data, analyze results, or draw scientific conclusions. The authors have reviewed and edited the final output and take full responsibility for the content of the manuscript.

Author's contributions

Conceptualization and Supervision: , Methodology: Investigation, Writing – original draft, and Writing – review & editing: All authors; Data collection: S.S; Data analysis: S.S; Funding acquisition and Resources: S.S.

6. References

1. Javan MB, Soltani A, Azmoodeh Z, Abdolahi N, Gholami N. A DFT study on the interaction between 5-fluorouracil and B12N12 nanocluster. RSC Adv. 2016;6(106):104513-21. (DOI: 10.1039/C6RA18196A)
2. Soliman KA, Aal SA. Theoretical investigation of favipiravir antiviral drug based on fullerene and boron nitride nanocages. Diam relat mater. 2021;117:108458. (DOI: 10.1016/j.diamond.2021.108458) (PMID: 34025036)
3. Bader RFW. Atoms in molecules. Acc chem res. 1985;18(1):9-15. (DOI:10.1021/ar00109a003)
4. Reed AE, Curtiss LA, Weinhold F. Intermolecular interactions from a natural bond orbital, donor-acceptor viewpoint. Chem rev. 1988;88(6):899-926. (DOI: 10.1021/cr00088a005)
5. Arabi Z, Gholami M, Zare K. Interaction of 5-fluorouracil with functionalized carbon nanotubes: a molecular dynamics simulation study. Sci rep. 2021;11(1):1-12. Link
6. Beheshtian J, Peyghan AA, Bagheri Z. DFT study of the interaction of 5-fluorouracil with BN nanotubes. J mol model. 2013;19(5):2197-203. (DOI: 10.1007/s00894-012-1751-2) (PMID: 23354475)
7. Li H, Heravi MR, Ebadi AG, Ahmadi S, Sarkar A. Study the nature of the interaction between 5-fluorouracil anti-cancer drug and zinc oxide nanocage. Braz j phys. 2022;52(2):53. (DOI:10.1007/s13538-022-01062-2)
8. Zhang L, Wang Y, Chen X. Molecular dynamics simulation of doxorubicin and camptothecin interactions with carbon nanotubes. J mol liq. 2023;345:117032. Link
9. Provin P, Khan M, Ahmadi S. Graphene as a carrier for doxorubicin drug delivery: a DFT study. Diam relat mater. 2023;132:109654. Link

10.Yousefi M, Rad MS, Shakibazadeh R, Ghodrati L, Kachoie MA. Simulating a heteroatomic CBN fullerene-like nanocage towards the drug delivery of fluorouracil. Mol simul. 2022;48(14):1284-92. (DOI:10.1080/08927022.2022.2086252)
11.Ciofani G, Danti S, D'Alessandro D, Moscato S, Menciassi A. Boron nitride nanotubes: biocompatibility and potential spill-over in nanomedicine. Small. 2010;6(21):2400-7. (DOI: 10.1002/smll.201201315) (PMID: 23423826)
12.Ferreira TH, Neves MC, Sousa EM, Soares DC. Boron nitride nanotubes in nanomedicine: functionalization and applications. Nanomedicine. 2015;10(16):2595-610. Link
13.Li R, Wang Y. Modification of boron nitride nanocages by titanium doping results unexpectedly in exohedral complexes. Nat commun. 2019;10(1):4908. (DOI: 10.1038/s41467-019-12877-0) (PMID: 31659166)
14.Yang X, Zhou S, Huang S, Zhao J. Metal-encapsulated boron nitride nanocages for solar-driven nitrogen fixation. J phys chem c. 2020;124(43):23798-806. (DOI:10.1021/acs.jpcc.0c07968)
15.Esrafili MD, Nurazar R. A comparative DFT study on the interaction of 5-fluorouracil with B12N12 and Al12N12 nanocages. J mol graph model. 2018;82:158-64. Link
16.Shariat M, Khodabakhshi MR. DFT investigation of 5-fluorouracil adsorption on boron nitride nanocages. J nanostruct chem. 2019;9(3):251-60. Link
17.Nejati K, Rezvani Z, Seyedahmadian E. A DFT study on the interaction of uracil and its derivatives with B12N12 nanocage. J mol liq. 2020;314:113654. Link
18.Sedighi M, Noori M, Shamlouei A. Computational study of drug delivery systems based on boron nitride nanocages. J mol struct. 2022;1258:132650. Link
19.Diznab HA, Javan MB, Soltani A, Gharibzadeh F. A comparative DFT study on the interaction of anticancer drugs with boron nitride nanocages. Appl surf sci. 2022;585:152624. Link
20.Fan X, Li Z. Adsorption of 5-fluorouracil on boron nitride nanocages: a DFT study with solvent effects. J Mol Liq. 2021;328:115432. Link
21.Longley DB, Harkin DP, Johnston PG. 5-fluorouracil: mechanisms of action and clinical strategies. Nat rev cancer. 2003;3(5):330-8. (DOI: 10.1038/nrc1074) (PMID: 12724731)
22.Heidelberger C, Chaudhuri NK, Danneberg P, Mooren D, Griesbach L, Duschinsky R, et al. Fluorinated pyrimidines a new class of tumour-inhibitory compounds. Nature. 1957;179(4561):663-6. (DOI: 10.1038/179663a0) (PMID: 13418758)
23.Pałasz A, Cież D. In search of uracil derivatives as bioactive agents. Uracils and fused uracils: Synthesis, biological activity and applications. Eur j med chem. 2015;97:582-611. (DOI: 10.1016/j.ejmech.2014.10.008) (PMID: 25306174)
24.Patra JK, Das G, Fraceto LF, Campos EV, Rodriguez-Torres MD, Acosta-Torres LS, et al. Nano based drug delivery systems: recent developments and future prospects. J nanobiotechnology. 2018;16(1):1-33. (DOI: 10.1186/s12951-018-0392-8) (PMID: 30231877)
25.Mu W, Chu Q, Liu Y, Zhang N. A review on nano-based drug delivery system for cancer chemoimmunotherapy. Nano-micro lett. 2020;12(1):142. (DOI: 10.1007/s40820-020-00482-6) (PMID: 34138136)
26.Sultana A, Zare M, Thomas V, Kumar TS, Ramakrishna S. Nano-based drug delivery systems: Conventional drug delivery routes, recent developments and future prospects. Med drug discov. 2022;15:100134. (DOI: 10.1016/j.medidd.2022.100134)
27.Wang X, Zhi C, Weng Q, Bando Y, Golberg D. Boron nitride nanotubes: synthesis, properties and applications. Nanoscale. 2018;10(33):15473-95. Link
28.Kim JH, Kim MJ, Park JY. Boron nitride nanotubes: a review of recent progress on biomedical applications. Nanomaterials. 2020;10(7):1360. Link
29.Golberg D, Bando Y, Huang Y, Terao T, Mitome M, Tang C, et al. Boron nitride nanotubes and nanosheets. ACS nano. 2010;4(6):2979-93. (DOI: 10.1021/nn1006495) (PMID: 20462272)
30.Khosravi A, Baei MT, Sayyed-Alangi SZ, Tazikeh Lemeski E. DFT-guided design of hydroxytyrosol-encapsulated nanocages: comparative insights into boron nitride versus carbon fullerenes for targeted drug delivery and therapeutic applications. *Adv theory simul*. 2025. Link
31.Rahimi M, Wali AF, Talath S, Aljasser A, Aldurdunji MM, Alqahtani F, et al. DFT investigation of iron-doped boron nitride nanoparticles for anastrozole drug delivery and molecular interaction. *Sci rep*. 2025;15(1):8670. (DOI: 10.1038/s41598-025-92888-8) (PMID: 40082535)
32.Moumivand A, Naderi F, Moradi O, Makiabadi B. Smart drug delivery: a DFT study of C_{24} fullerene and doped analogs for pyrazinamide. *Nanoscale adv*. 2025;7(5):1287-1299. (DOI: 10.1039/D4NA00560K) (PMID: 39802333)
33.Guo L, Chen C, Luo Y, Zuo K, Guo Z, Tang D. Theranostic potential of metal-doped $B_{36}N_{36}$ nanocages for β-lapachone delivery: A density functional theory study. *J mol liq*. 2025. Link
34.Opi MH, Ahmed T, Swarna MR, Piya AA, Shamim SUD. Assessment of the drug delivery potential of graphene, boron nitride and their in-plane doped structures for hydroxyurea anti-cancer drug via DFT study. *Nanoscale Adv*. 2024;6(20):5042-5054. (DOI: 10.1039/D4NA00428K) (PMID: 39148501)
35.Saha SK, Nishat M, Mostofa MR, Hasnat MA, Al-Amin. The adsorption effect of an anti-diabetic drug on the surface of $B_{12}N_{12}$ and $XB_{11}N_{12}$ (X = Ga, Al, In) nanocages: A comparative DFT study with COSMO insights. *Chem phys lett*. 2025;878:142332. (DOI: 10.1016/j.cplett.2025.142332)